Electronic Journal of Structural Engineering

Original Article

Cite this: DOI:10.56748/ejse.24805

Received Date: 14 April 2025
Accepted Date: 22 December 2025

1443-9255
https://ejsei.com/ejse

Optimization of Large-Span Spatial Building Structures Based on Kalman Filter and Improved Genetic Algorithm

Xiangfeng Chen [a*], Jianjun Xu [b]

[a] College of Civil Engineering, Longdong University, Xifeng, 745000, China
[b] Engineering Project Department of the Second Oil Production Plant of Changqing Oilfield, Qingcheng, 745100, China
*Corresponding author: chenxiangfeng8763@126.com

Abstract

Large-span spatial building structures are complex and face challenging environments after construction. Under external impacts, vibrations, and wind and snow loads, certain structural components may undergo deformation. Therefore, it is crucial to implement spatial building structure optimization during the construction process. This study proposes an optimization model for large-span spatial building structures by integrating Genetic Algorithm, Kalman Filter, Influence Matrix, and Particle Swarm Optimization. Experimental results show that the proposed algorithm achieves the lowest tracking frequency and phase mean square error, with a loop convergence time of only 0.3s and a frequency tracking error of 15Hz. In practical applications, the optimized cable force values are reduced by an average of 61kN compared to the original values, and the average bending stress decreases by 5.9MPa. The mean error of model-reconstructed displacement is 3.3% and 3.8%, achieving the highest reconstruction accuracy. The experimental data demonstrate that the proposed model exhibits superior performance in real-world optimization, contributing to large-span spatial building structures by ensuring safety and improving construction efficiency.

Keywords

Genetic algorithm, Kalman filter, Artificial neural network, Influence matrix, Particle swarm optimization, Large-span spatial

1. Introduction

With the steady growth of the global economy and increasing social and cultural activities, the demand for large-span spatial structures continues to rise (Su et al., 2025). The performance of large-span spatial structures, especially those relying on cable systems (such as cable trusses, cable-supported domes, tensioned beams, etc.), is highly dependent on the initial state and service response of key components (such as cables). This type of structure faces several prominent engineering challenges and urgently needs precise and efficient optimization methods. High cable force sensitivity is a common challenge. Even minor changes in cable force can lead to significant alterations in structural displacement and internal force distribution and even trigger unexpected large deformations or instability risks (Yin et al., 2022). Traditional design methods rely on empirical estimation and simplified analysis, making it difficult to accurately capture this sensitivity, resulting in the difficulty of precisely controlling the structural safety margin or causing material waste. Adapting to complex dynamic environments is also a major challenge. Structures face complex and time-varying load conditions during the construction phase (such as step-by-step tensioning and lifting) and the operation phase (such as wind loads, crowd loads, and temperature changes). These dynamic environments require real-time perception and prediction of the structural state in order to adjust the control strategy in a timely manner or assess the safety status (Ledong et al., 2022). However, structural optimization needs to simultaneously consider safety (such as controlling displacement and stress), economy (such as minimizing material usage and cable force), and construction feasibility (such as tensile force limit and adjustment step sequence), and there is a strong nonlinear coupling relationship among the variables, making the solution difficult. When dealing with such large-scale, nonlinear and multi-objective optimization problems, the existing methods often face the predicaments of low computational efficiency, being prone to falling into local optimum or having difficulty meeting the real-time requirements. It is precisely these specific challenges, namely the extreme sensitivity to minor changes in cable force, the need for real-time state estimation under complex dynamic loads, and the complexity of strong nonlinear multi-objective optimization, that constitute the fundamental driving force for the research to seek more advanced optimization methods. Kalman Filter (KF) can process dynamic data in real time, effectively suppress noise, and integrate multi-source data to achieve accurate variable estimation (Owen et al., 2023). Genetic Algorithm (GA) has strong global search capabilities, enhances search efficiency through population parallelism, and continuously optimizes structural design based on fitness evaluation (Ghannadi et al., 2023). Therefore, this study develops an optimization model for large-span spatial structures based on KF and GA. The model incorporates Artificial Neural Network (ANN) to improve GA, enabling rapid global optimization. KF is then applied to filter observation data. Additionally, Influence Matrix and Particle Swarm Optimization (PSO) are integrated to optimize cable forces, aiming to enhance the stability of large-span spatial structures, reduce engineering costs, and improve construction safety. This study innovatively combines KF and GA, introduces further algorithm improvements, and comprehensively considers various influencing factors during optimization to enhance the model's adaptability in dynamic and complex environments.

1.1 Related works

In the field of artificial intelligence, both KF and GA were developed to solve complex problems. They improve result accuracy and solution quality through information fusion and population evolution. Researchers worldwide have conducted extensive studies on these methods. For example, Zhao et al. (2022) developed a hybrid non-single-state fuzzy strong tracking Kalman Filter model to enhance state estimation performance in high-precision optoelectronic tracking systems under complex conditions. This model integrated strong tracking and fuzzy logic filtering techniques. Simulations and experimental comparisons demonstrated their significant advantages. Bakhshi's team (2023) addressed the oversight of simple architecture methods in flood warning systems by optimizing a Long Short-Term Memory model using KF for water flow forecasting. Simulations based on real dam daily flow sequences verified the feasibility and high performance of deep learning methods with simple architectures for flood prediction. Sohail (2023) explored the limitations of traditional optimization tools in engineering and data science when dealing with large-scale or high-dimensional data. He examined advanced GA applications, combining time-series forecasting, Bayesian inference, and GA, confirming their strong effectiveness in artificial intelligence. Khatri et al. (2023) proposed an efficiency improvement model for isolated hybrid energy systems based on GA to address the unpredictability of renewable energy growth. The model analyzed multiple factors, including input variables, energy costs, probability of energy loss, and renewable energy contributions, proving its superior performance. Ghezelbash et al. (2023) developed a genetic-based support vector machine model to tackle challenges in mineralization process transformation. They used traditional clustering algorithms to create mineral prospectivity maps and incorporated GA into the clustering process. Experimental results showed that this model outperformed similar alternatives.

Large-span spatial building structures emerged alongside societal advancements and have received significant research attention. For instance, Tian et al. (2024) addressed the poor fitting of existing force calculation methods for arch-cable structures. They proposed a multi-loop nested algorithm that decomposes the construction process into subsystem control modules, setting stress and displacement control indicators for each module. Results demonstrated that this algorithm effectively handled discreteness issues and provided greater parameter flexibility. Choi et al. (2023) tackled the high construction cost and environmental impact of prestressed concrete slabs by developing a multi-objective green design model. They used a non-dominated sorting GA to optimize input slab dimensions and loads, proving that their model reduced both construction costs and carbon emissions compared to existing slab design methods. Entezami and Sarmadi (2025) introduced an innovative machine learning-assisted prediction method to address the vulnerability of large-span suspension bridges to storm-induced vibrations. Their method integrated metric learning, kernel learning, and hybrid learning into a unified regularization framework, demonstrating its effectiveness and practicality. Yu et al. (2023) aimed to improve the computational efficiency of force optimization in suspension cables, which often involves extensive matrix operations. They proposed a new cable force optimization method that combined finite element analysis with multi-objective optimization. Results indicated that this method significantly improved optimization efficiency. Doroudi et al. (2024) tackled data processing and feature selection challenges in large-span bridges. They proposed an observer-teacher-learner-based optimization method, using wavelet transform and multivariate empirical mode decomposition to extract time-domain features. Their results confirmed that this method made significant contributions to structural health monitoring.

In summary, although researchers worldwide have made progress in studying large-span spatial structures, existing studies often fail to consider all influencing factors, leading to discrepancies between computational results and real-world performance. Therefore, this study combines KF and GA, utilizing GA for global search and optimization while applying KF for real-time dynamic data processing. This approach enhances optimization efficiency and accuracy, improves structural stability, and significantly reduces engineering costs.

2. Optimization model construction for large-span spatial engineering

2.1 Improved GA design with ANN

The core structural problems faced by large-span spatial structures during construction and service are their extreme sensitivity to mechanical behavior, strong nonlinearity, and adaptability to complex environments. Minor changes in internal forces of key components may lead to significant or even disproportionate redistribution of overall displacement and internal force distribution of the structure, resulting in unpredictable risks of large deformation or instability. The structure is subjected to complex and time-varying dynamic load environments during the construction and operation phases, requiring real-time perception and prediction of the structural state. In large-span engineering optimization, GA effectively searches for the global optimal solution and adapts to complex forces. This study uses GA to determine the dynamic noise covariance matrix. GA is an optimization algorithm inspired by biological evolution. By simulating processes such as natural selection, crossover, and mutation, GA iteratively searches for possible solutions (Lee et al., 2024). The flowchart of GA is shown in Fig. 1.

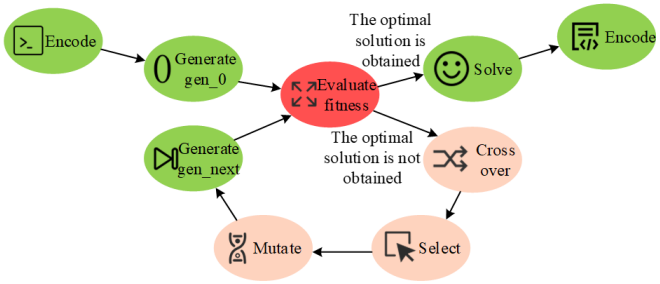

Fig. 1 Schematic diagram of GA process

As shown in Fig. 1, the problem parameters are first encoded to generate the initial population. Each individual's fitness is then evaluated to measure its ability to solve the problem. In the selection process, individuals are chosen based on their fitness. The selected individuals undergo crossover, exchanging gene segments to produce new individuals. Meanwhile, some individuals undergo mutation to increase population diversity, generating the next generation. The new population enters the fitness evaluation stage, and this iteration continues until a satisfactory solution is found. In the selection phase, the probability of an individual being selected for reproduction is proportional to its fitness, as shown in Equation (1).

$$p_i = \frac{f(a_i)}{\sum_{j=1}^{n} f(a_j)} \tag{1}$$

In Equation (1), a represents a vector encoding an individual's characteristics, p represents the probability of being selected, f denotes fitness, n is the total number of individuals, i and j represent individuals in n. In the crossover phase, the selected individuals generate offspring through the crossover operation, as expressed in Equation (2).

$$a' = (a_{i1}, a_{i2}, \ldots, a_{ik}, a_{j(k+1)}, \ldots, a_{jn}) \tag{2}$$

In Equation (2), a' represents the offspring of a. A small probability is applied to modify certain genes in the new individuals, introducing mutations to increase population diversity. The mutation operation is expressed in Equation (3).

$$a''_{nk} = a_{nk} + \delta, with probability \mu \tag{3}$$

In Equation (3), a'' represents the mutated gene, μ denotes the mutation rate, and δ represents a small random variation. By continuously repeating these steps, GA gradually improves solution quality over multiple generations, approaching the optimal solution. However, GA encounters challenges in optimizing complex problems, such as large search spaces and local optima. ANN has strong learning capabilities and can leverage its fast-learning ability to guide GA, enhancing search efficiency (Xiong et al., 2024). The flowchart of ANN-GA is shown in Fig. 2.

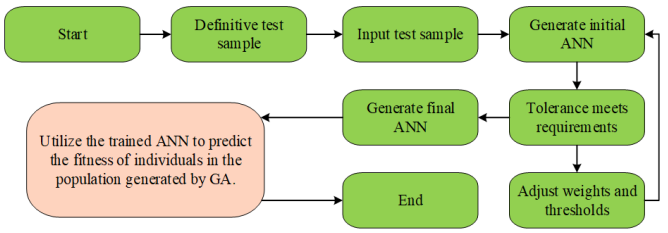

Fig. 2 Schematic diagram of ANN-GA workflow

As shown in Fig. 2, trial samples are randomly selected and input into the ANN prediction model for learning. The initial model is then generated and subjected to tolerance analysis. If the tolerance meets the requirements, the final ANN model is generated, otherwise, weights and thresholds are adjusted. GA's initial parameters are then set, and the ANN model is integrated to generate the optimal prediction model. Next, relevant constraints and optimization objectives are established. Fitness values are computed, and if the termination criteria are met, the final result is output. If not, individuals are selected from the parent generation, and new populations are generated through crossover and mutation. The process returns to the GA initialization step and iterates until the termination criteria are satisfied.

2.2 Algorithm design integrating KF and ANN-GA

When the deformation of a large-span spatial structure exceeds its limit, safety accidents may occur, making structural optimization essential. Based on a discretized linear stochastic system, future responses can be predicted. The state vector of the observation point is expressed in Equation (4).

$$Y(t) = [y(t), \dot{y}(t)]^T \tag{4}$$

In Equation (4), Y represents the state vector, t denotes the current time, y represents the system state vector, $\dot{y}$ is the derivative of y, and T is the transpose process. The state equation is formulated as shown in Equation (5).

$$\dot{Y}(t) = \begin{bmatrix} 0 & 1 \\ 0 & 0 \end{bmatrix} Y(t) + \begin{bmatrix} 0 \\ 1 \end{bmatrix} \omega(t) \tag{5}$$

In Equation (5), $\dot{Y}$ is the derivative of Y, and ω represents the noise vector. The state equation is solved as shown in Equation (6).

$$Y(t) = \begin{bmatrix} 0 & t - t_0 \\ 0 & 1 \end{bmatrix} Y(t_0) + \int_{t_0}^{t} \begin{bmatrix} 1 & t - \alpha \\ 0 & 1 \end{bmatrix} \begin{bmatrix} 0 \\ 1 \end{bmatrix} \omega(\alpha) d\alpha \tag{6}$$

In Equation (6), t_0 is the initial time, α is the integration variable, and $d\alpha$ represents the differential of α. KF is constructed based on a discretized linear stochastic system. It can estimate structural states in real-time with high accuracy, making it more suitable for large-span engineering optimization. This algorithm updates states estimates by combining the previous estimate with the current observation using the minimum mean square error criterion (Huang et al., 2024). The flowchart and filtering effect of KF are shown in Fig. 3.

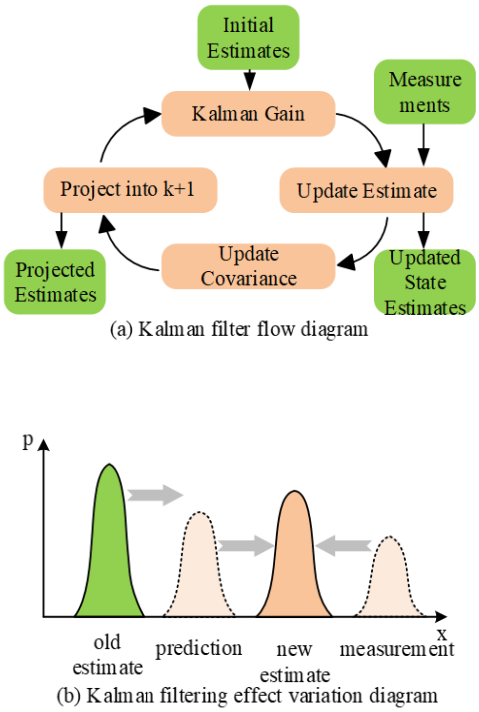

Fig. 3 KF workflow and filtering effect diagram

As shown in Fig. 3(a), the system state and covariance are first initialized. The actual measurement value is then obtained and used to compute the Kalman gain, determining the weight distribution between the predicted and measured values. Using the computed Kalman gain, the prediction and measurement values are combined through the update step to obtain an updated state estimate. Covariance is updated to reflect estimation uncertainty. The updated state is then projected onto the next step (k+1) to predict the estimate, and the process enters the next iteration. As shown in Fig. 3(b), KF continuously corrects state estimates. It starts with an initial probability distribution, predicts based on the previous estimate, and combines it with the probability distribution of new measurements to obtain an updated estimate. The state prediction equation of KF is shown in Equation (7).

$$x_k = Fx'_{k-1} + Bu_k \tag{7}$$

In Equation (7), k and $k-1$ represent time, u denotes the control input vector, B represents the control input matrix, F is the state transition matrix, x is the prior state estimate, and x' is the posterior state estimate. The error covariance prediction equation is shown in Equation (8).

$$P_k = FP_{k-1}F^T + Q \tag{8}$$

In Equation (8), P represents error covariance, F^T is the transpose matrix of F, and Q represents the process noise covariance matrix. The next step involves updating the state variable estimate. First, the Kalman gain is calculated as shown in Equation (9).

$$K_k = P_k H^T (HP_k H^T + R)^{-1} \tag{9}$$

In Equation (9), H^T represents the transpose matrix of observation matrix H, K represents the gain matrix, and R is the covariance matrix of observation noise. The state update equation is shown in Equation (10).

$$x_k{}' = x_k + K_k(z_k - Hx_k) \tag{10}$$

In Equation (10), z represents the measurement, and $x_k{}'$ is the posterior state estimate at time k. The error covariance update equation is shown in Equation (11).

$$P'_k = (I - K_k H)P_k \tag{11}$$

In Equation (11), I is the identity matrix, and P' is the posterior error covariance. During the initialization of KF, the state noise covariance matrix plays a crucial role. Based on the KF principle, a deformation detection model is established, incorporating an improved ANN-GA approach. The specific process is shown on Fig. 4.

As shown in Fig. 4, GA is first used to generate an initial population of deformation detection parameter combinations. ANN is then used to predict the fitness of individuals in the population, reflecting the effectiveness of parameter combinations in deformation detection. Individuals with low fitness are eliminated, and new populations are generated through genetic operations such as crossover and mutation. This process continues until an optimal parameter combination is obtained. The optimized results are input into the KF module, where updating, gain, and prediction functions optimize the detection data to obtain filtered results. This process integrates the advantages of ANN, GA, and KF, significantly improving deformation detection quality and efficiency.

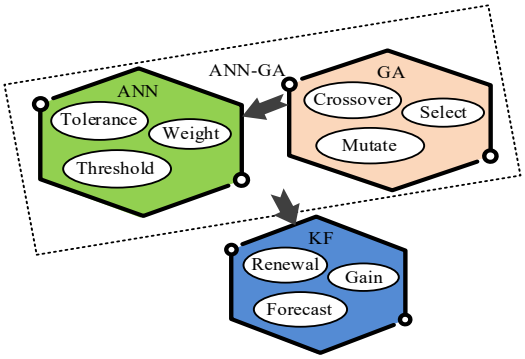

Fig. 4 ANN-GA innovation Kalman filter process diagram

2.3 Optimization model for building structures based on deformation detection

In large-span structural optimization, in addition to optimizing deformation monitoring, cable force optimization in cable-rod systems is also crucial. It ensures structural safety and adaptability to complex loads. The influence matrix method is commonly used for cable force optimization. It constructs a matrix based on the relationship between structural response and cable force, determining the reasonable bridge completion cable force and solving construction cable tension (Bel Hadj Ali et al., 2022). The vector relationship is first established as shown in Equation (12).

$$Ax = D \tag{12}$$

In Equation (12), A represents the influence matrix, while x and D represent the applied and adjusted vectors, respectively. The equations for calculating bending moment, axial force, shear force, and displacement are shown in Equation (13).

$$\begin{cases} M = M_p + A_M T \\ F = F_p + A_F T \\ Q = Q_p + A_Q T \\ Z = Z_p + A_Z T \end{cases} \tag{13}$$

In Equation (13), M represents the bending moment of the structural section, P is the dead load effect, A is the influence matrix, and T represents the cable force vector. F, Q, and Z denote axial force, shear force, and displacement, respectively. The cable-rod system in large-span structures is often highly nonlinear and multi-variable, requiring a global optimal solution. The study incorporates an improved PSO to handle various constraints, aiding in the search for the optimal cable force. The core idea of PSO is inspired by bird foraging behavior, utilizing individual information sharing within a group to explore different regions in search of optimal solutions (Pham et al., 2025). The velocity and position update equations for particles in space are shown in Equation (14).

$$\begin{cases} v_{id}(k+1) = \omega v_{id}(k) + c_1 r_1 [pbest_{id}(k) - x_{id}(k)] + c_2 r_2 [gbest_{id}(k) - x_{id}(k)] \\ x_{id}(k+1) = x_{id}(k) + v_{id}(k+1) \end{cases} \tag{14}$$

In Equation (14), k represents the number of iterations, v denotes the particle velocity, x indicates the position, ω is the inertia factor, c represents the constant acceleration, and r is a random number. $gbest$ stands for the individual best value, while $pbest$ represents the global best value. In optimization problems, constraint conditions for parameter variables generally include equality constraints and inequality constraints. To ensure the optimization results satisfy these conditions, constraints are often incorporated into the objective function as penalty functions. The penalty factor in the penalty function is a large positive number, which penalizes constraint violations. Taking structural strain energy as an example, the structure is first discretized into multiple elements. Based on the bending moment, axial force, and sheer force of each element, strain energy is calculated by considering material and geometric parameters. By minimizing strain energy, cable force optimization is achieved. Other objective functions follow a similar approach, where minimizing the corresponding index leads to cable force optimization. The optimization process combining PSO and the influence matrix method is shown in Fig. 5.

As shown in Fig. 5, the process begins with problem analysis and data preparation, where the optimization objective is clarified, and constraints such as cable force ranges are defined. The study used ANSYS finite element analysis software to construct an accurate structural model, in order to obtain the relationship between structural response and cable force. A decision is then made on whether to use the influence matrix method or PSO for optimization. Next, in the influence matrix method,

adjustment and response vectors are defined, and influence coefficients are computed to form the influence matrix. Simultaneously, PSO is initialized, where particle encoding is performed for cable forces, and parameters such as swarm size are set. The iterative optimization process then begins, calculating particle fitness and updating particle velocity and position based on the equations. Finally, results are evaluated and output. When the termination conditions are met, the optimal cable force distribution is obtained and applied to design or construction. The ANN-GA innovation Kalman filter is used for deformation monitoring, while PSO and the influence matrix method are applied for cable force optimization. This approach establishes an optimization model for large-span spatial structural engineering. The optimization model framework developed in this study is shown in Fig. 6.

As shown in Fig. 6, displacement sensors and strain gauges are first used to collect deformation data under different conditions. After noise reduction and normalization preprocessing, network parameters are determined, and ANN is trained. The trained ANN is then used to optimize GA parameters, improving prediction accuracy. The optimized predicted values and actual measurements are input into the innovation Kalman filter for deformation monitoring optimization. Simultaneously, cable force optimization is carried out using the influence matrix method or PSO. Finally, the information is integrated into output optimization results, achieving the goal of optimizing large-span spatial structural engineering.

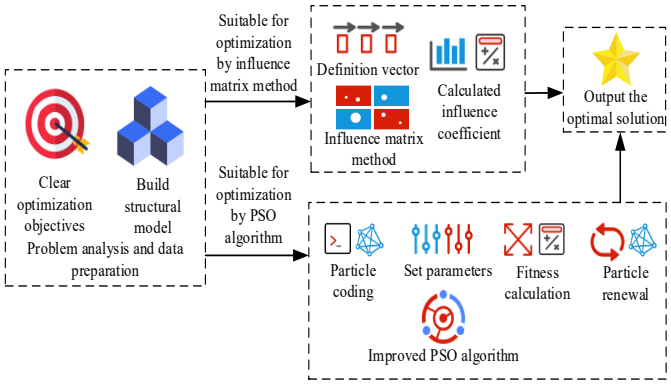

Fig. 5 Cable force optimization process combining PSO and influence matrix method

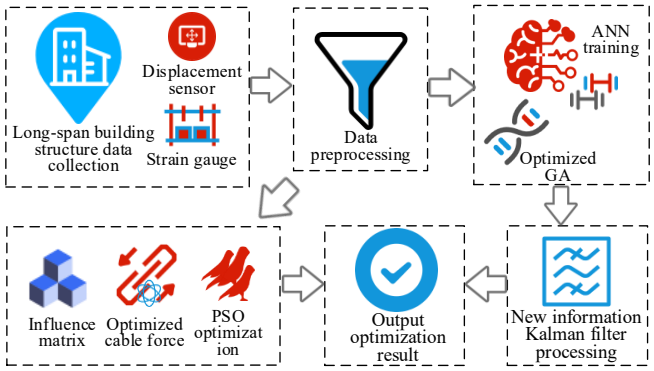

Fig. 6 Workflow diagram of the constructed optimization model

3. Experimental analysis of the optimization model for large-span spatial engineering

3.1 Performance verification of the improved algorithm

To verify the performance advantages of the ANN-GA innovation KF, this study conducted comparative experiments with the traditional KF, Extended Kalman Filter (EKF), and Cubature Kalman Filter (CKF). The experiments were performed on a system equipped with an Intel Core i3-6100 CPU, 16GB of memory, and 512GB of storage, using Python 3.6 on Windows 10. Simulated data were generated in MATLAB, with an input frequency of a 500Hz initial Doppler signal. The simulation data utilizes representative dynamic models of large-span spatial structures, known for exhibiting significant geometric nonlinearity and sensitivity to dynamic inputs. The core input signal simulates an initial Doppler frequency of 500 Hz, intentionally chosen to represent the complex vibration modes that may be encountered in this structure. The signal is contaminated by additional thermal noise, with a signal-to-noise ratio range of -22 dB to -15 dB. This range is specifically selected to replicate the challenging noise and interference conditions commonly present in the operating environments of real-world buildings and large-span structures. Therefore, the simulated data simulated the dynamic response of key structural points that are highly sensitive to external stimuli. The frequency tracking error comparison is shown in Fig. 7.

As shown in Fig. 7(a), the proposed algorithm achieved a loop convergence time of 0.3s, with a frequency tracking error of 15Hz. In contrast, KF exhibited significant fluctuations and only stabilized after 1.3s, ultimately reaching a tracking frequency error of 32Hz. As shown in Fig. 7(b), both EKF and CKF converged within 1s. However, EKF had a higher final tracking error than CKF, measuring 28Hz and 25Hz, respectively. These results indicated that the proposed algorithm provided a significant improvement in tracking performance compared to traditional algorithms. To further evaluate the tracking performance under different Signal-to-Noise Ratio (SNR) conditions, the system was tested with thermal noise SNR ranging from -22dB to -15dB. The Mean Square Errors (MSE) of loop frequency and phase tracking are shown in Fig. 8.

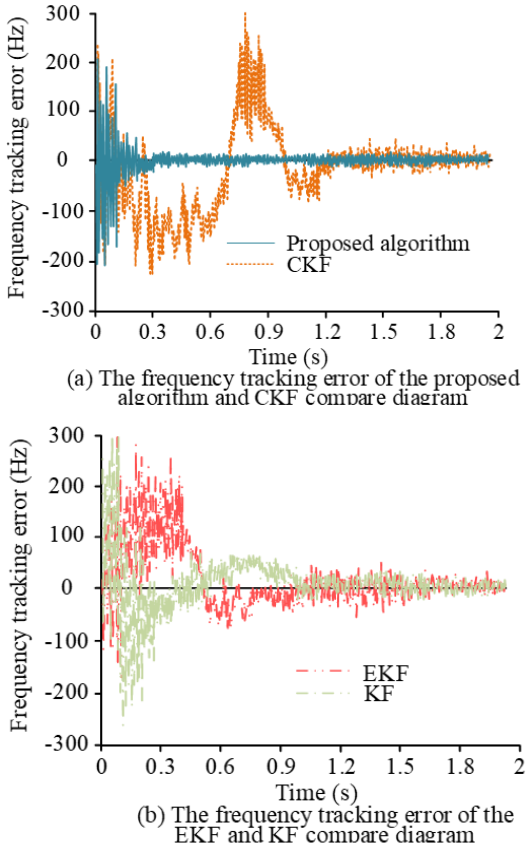

Fig. 7 Comparison of frequency tracking errors of different algorithms

As shown in Fig. 8(a), the MSE of frequency tracking decreased continuously with increasing SNR for all four algorithms. EKF exhibited the largest decrease in tracking frequency errors as the SNR increased, reaching a minimum of 1.8Hz at -15dB. The proposed algorithm maintained the lowest tracking frequency error among all algorithms, measuring only 0.8Hz at -15dB. As shown in Fig. 8(b), the phase tracking error also decreased as SNR increased. After a 7dB increase in SNR, KF's phase tracking error decreased by 0.09rad, while EKF and CKF decreased by 8rad. The proposed algorithm showed the smallest decrease at 0.06rad but remained the most stable among all four algorithms. These results demonstrated the superior robustness of the proposed algorithm. To further verify its filtering effectiveness, the study compared the fitness values of different algorithms during the iteration process and evaluated the filtered coordinate values against actual monitoring data, as shown in Fig. 9.

As shown in Fig. 9(a), after 50 iterations, the proposed algorithm stabilized, with the best fitness value reaching 20. Although EKF achieved a fitness value of 15, second only to the proposed algorithm, it did not stabilize until 250 iterations. CKF converged after 170 iterations, with the best fitness value of 13, while KF stabilized after 210 iterations, with the best fitness value of 10. As shown in Fig. 9(b), compared to the actual monitoring data, the proposed algorithm was closest to the real values in the eighth monitoring period, with an average coordinate deviation of only 0.2mm. KF deviated the most, with an average coordinate difference of 0.6mm. These results demonstrated the feasibility of the proposed algorithm in filtering applications.

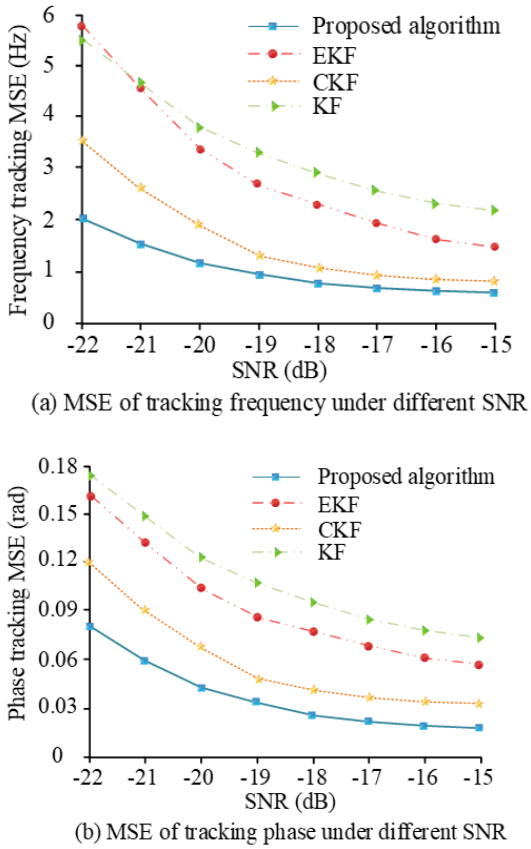

Fig. 8 Frequency and phase mean square error results.

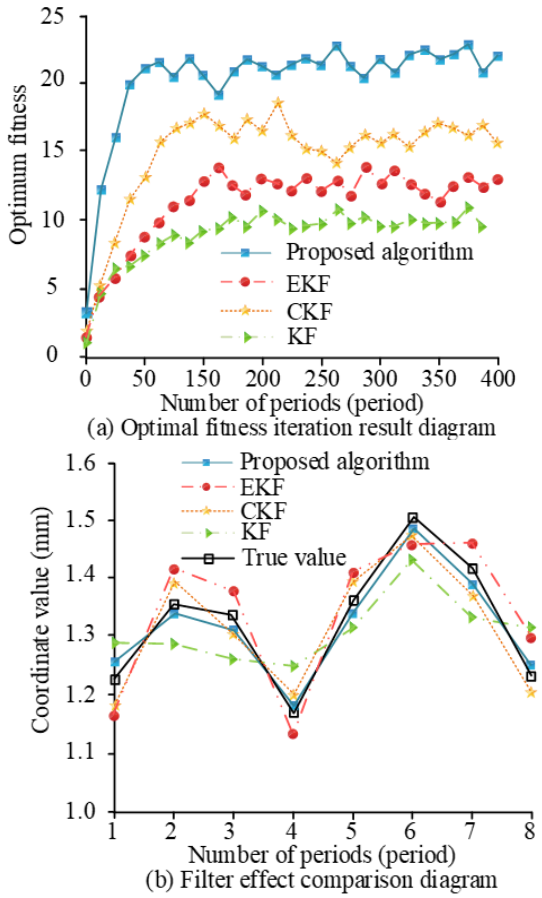

Fig. 9 Filtering effects of different algorithms

3.2 Performance verification of the optimization model

After verifying the superiority of the proposed algorithm, its practical applicability was further evaluated by comparing it with the Tabu Search-Artificial Neural Network (TS-ANN) model, the Particle Swarm Optimization-Finite Element Method-Filtering Algorithm (PSO-FEM-FA) model, and the Genetic Algorithm-Simulated Annealing Algorithm (GA-SA) model. The experimental data comes from the long-term health monitoring system of a large spatial structure project with a span of 120m in a large manufacturing factory. The system continuously collected cable force and stress-strain data for 6 months through force sensors and strain gauges installed on key cables and nodes, with a cumulative effective data volume of about 15GB, providing sufficient real physical observation sequences for model comparison. The processing and analysis of data were carried out in the hardware and software environments configured in Table 1. The specific experimental environment is listed in Table 1.

Table 1. Experimental environment and configuration

Experimental environment	Category	Configuration
Hardware configuration	Internal memory	DDR4 8GB
	Video memory	4GB Nvdia Geforce GTX1050Ti
	CPU	Intel Core i5-7300, 2.50GHz
	Graphics card	Nvdia Geforce GTX1050Ti
	Operating system	Windows 10
Software environment	Python	3.6
	MATLAB	2018b

In order to evaluate the optimization effect of different models on the tension of inclined cables, this study conducted on-site testing on a 120m span steel roof structure in the large single-layer manufacturing factory mentioned above and closely monitored the key section of 60m long near the mid span. The choice of a 120m span is due to its typical representativeness in large-span spatial structures, which can fully reflect the geometric nonlinear behavior and cable force redistribution effect of the structure under complex loads. The key section of 60m long near the mid span is tested because it has clear stress and typical boundary conditions, which can effectively reflect the continuous distribution law of cable force optimization along the length of the component. The comparison results are shown in Fig. 10.

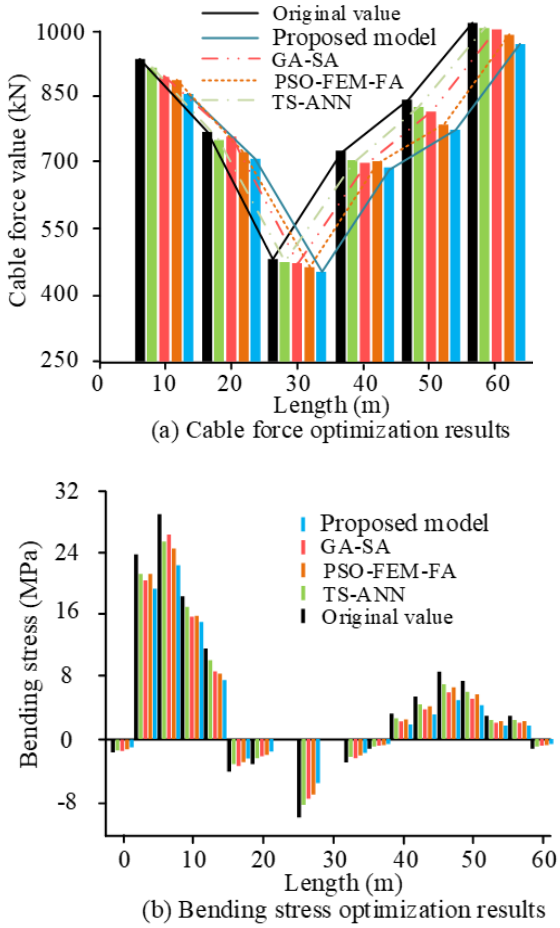

Fig. 10 Cable force optimization effect diagram

As shown in Fig. 10(a), the TS-ANN model exhibited varying degrees of cable force reduction depending on the length, with the maximum reduction reaching 31kN at 40m and an average reduction of 25kN. The GA-SA model achieved similar optimization results to the TS-ANN model, with an average reduction of 29kN, but demonstrated lower optimization stability. The proposed model and the PSO-FEM-FA model showed more significant optimization effects, reducing cable force by 61kN and 46kN,

respectively. As shown in Fig. 10(b), the TS-ANN and GA-SA models demonstrated limited optimization effects on bending stress, reducing stress by only 2.6MPa and 2.9MPa, respectively. In contrast, the proposed model and the PSO-FEM-FA model achieved greater reductions. The proposed model showed the most significant reduction, reaching 7MPa at 8m and averaging a reduction of 5.9MPa. The PSO-FEM-FA model followed, with an average stress reduction of 4.6MPa. To further compare the effectiveness of the four models in reconstructing deformation displacement under different working conditions, strain measurement errors were set at 5% and 15%, and the results are shown in Fig. 11.

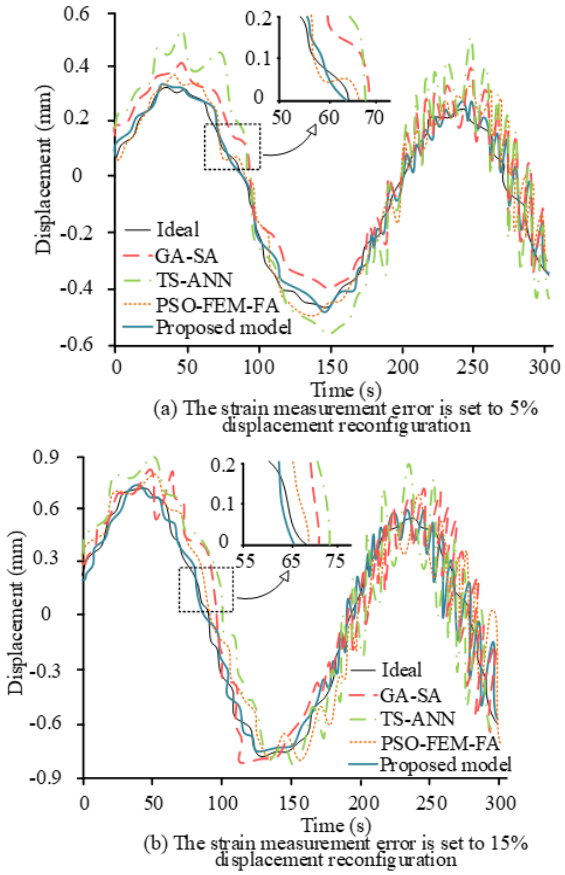

Fig. 11 Deformation displacement reconstruction results under different errors

As shown in Fig. 11(a), when the strain measurement error was 5%, the proposed model was closest to the ideal reconstructed displacement curve, with an average error of 3.3%. The PSO-FEM-FA model followed, with an average error of 6.9%. The TS-ANN model deviated the most from the ideal curve, with the highest average error of 38.9%. As shown in Fig. 11(b), when the strain measurement error increased to 15%, the proposed model remained the closest to the ideal curve, with only a 0.5% increase in average error. In contrast, the TS-ANN model's average error increased by 10.2% to 49.1%. Although the PSO-FEM-FA model remained relatively close to the ideal curve, its average error increased by 6.8% under 15% strain measurement error. These experimental results indicated that the proposed model demonstrated superior performance in reconstructing deformation displacement and exhibited higher robustness.

4. Conclusion

Large-span spatial structures have become a key choice for landmark urban buildings due to their unique advantages. These structures feature large spans and diverse forms while bearing significant responsibilities in public safety and social functionality. Therefore, optimizing their structural performance is crucial for advancing the construction industry and meeting urban development needs. This study introduced an improved approach based on KF and GA, leveraging the real-time accurate state estimation of KF and the global search capability of GA to enhance deformation monitoring. Additionally, the study incorporated an influence matrix and PSO to optimize structural cable forces. Experimental results showed that the proposed algorithm achieved a loop convergence time of 0.3s and a frequency tracking error of 15Hz. Among the four compared algorithms, it consistently maintained the lowest root mean square errors for both frequency and phase tracking. When the SNR was -15dB, the frequency tracking error was only 0.8Hz, and the phase tracking error was 0.02rad. In practical applications, the proposed model demonstrated significant effectiveness in optimizing cable forces, with an average reduction of 61kN compared to the original values, while the average bending stress decreased by 5.9MPa. Under strain measurement errors of 5% and 15%, the reconstructed displacement errors averaged 3.3% and 3.8%, respectively, showing minimal variation as strain measurement errors increased. Overall, the contribution of the research method lies in that its cable force optimization results directly reduce the working stress level of key load-bearing components, effectively alleviate the potential overload risk of the structure under complex load combinations, and provide additional margin for the structural safety reserve. The average reduction of bending stress significantly reduces the stress concentration phenomenon in key parts. This not only improves the bearing capacity of local components, but more importantly reduces the possibility of buckling instability of the structure as a whole under extreme loads. By optimizing the cable force distribution and reducing the bending stress, this model enhances the overall stiffness and stability of the structure. It is expected to improve its vibration characteristics under wind loads and dynamic loads and enhance the applicability and long-term service performance of the structure. The optimized deformation displacement reconstruction accuracy provides a more reliable database for structural health monitoring and condition assessment, directly serving the safe operation and maintenance of the structure. Although the proposed algorithm and model showed performance advantages in multiple aspects, the experimental scenarios were limited, and the generalization capability of the model remains insufficiently validated. Future research should expand experimental dimensions and integrate additional algorithms to further enhance model performance.

Fundings

The research is supported by: Qingyang Science and Technology Plan Project, Study on Strength Characteristics and Influencing Factors of Tire Reinforced Construction Waste Soil, (No. QY-STK-2024B-166).

Reference

Bakhshi Ostadkalayeh, F., Moradi, S., Asadi, A., Moghaddam Nia, A., & Taheri, S. (2023). Performance improvement of LSTM-based deep learning model for streamflow forecasting using Kalman filtering. Water Resources Management, 37(8), 3111-3127. https://doi.org/10.1007/s11269-023-03492-2

Bel Hadj Ali, N., Aloui, O., & Rhode-Barbarigos, L. (2022). A finite element formulation for clustered cables with sliding-induced friction. International Journal of Space Structures, 37(2), 81-93. https://doi.org/10.1177/09560599221084597

Choi, J., Hong, D. H., Lee, S. H., Lee, H. Y., Hong, T., Lee, D. E., & Park, H. S. (2023). Multi-objective green design model for prestressed concrete slabs in long-span buildings. Architectural Engineering and Design Management, 19(5), 531-549. https://doi.org/10.1080/17452007.2022.2147897

Doroudi, R., Lavassani, S. H. H., & Shahrouzi, M. (2024). Damage detection for long-span bridges through support vector machine, wavelet transform, and multivariate empirical mode decomposition. International Journal of Structural Engineering, 14(2), 164-185. https://doi.org/10.1504/IJSTRUCTE.2024.138127

Entezami, A., & Sarmadi, H. (2025). Machine learning-aided prediction of windstorm-induced vibration responses of long-span suspension bridges. Computer-Aided Civil and Infrastructure Engineering, 40(8), 1043-1060. https://doi.org/10.1111/mice.13387

Ghannadi, P., Kourehli, S. S., & Mirjalili, S. (2023). A review of the application of the simulated annealing algorithm in structural health monitoring (1995-2021). Fracture and Structural Integrity, 17(64), 51-76. https://doi.org/10.3221/IGF-ESIS.64.04

Ghezelbash, R., Maghsoudi, A., Shamekhi, M., Pradhan, B., & Daviran, M. (2023). Genetic algorithm to optimize the SVM and K-means algorithms for mapping of mineral prospectivity. Neural Computing and Applications, 35(1), 719-733. https://doi.org/10.1007/s00521-022-07766-5

Huang, S., Liu, Z., Liu, X., Wang, Z., Li, X., & Tong, T. (2024). Experimental study and neural network predictions of early-age behavior of microexpansion concrete in large-diameter steel tube columns. Science of Advanced Materials, 16(9), 1006-1017. https://doi.org/10.1166/sam.2024.4702

Khatri, K. A., Shah, K. B., Logeshwaran, J., & Shrestha, A. (2023). Genetic algorithm-based techno-economic optimization of an isolated hybrid energy system. ICTACT Journal on Microelectronics, 8(4), 1447-1450. https://doi.org/10.21917/ijme.2023.0249

Ledong, Z., Cheng, Q., Yikai, S., & Qing, Z. (2022). Aerodynamic shape optimization emphasizing static stability for a super-long-span cable-stayed bridge with a central-slotted box deck. Wind and Structures, 35(5), 337-351. https://doi.org/10.12989/was.2022.35.5.337

Lee, S., Lee, J., Kim, M., Lee, S., & Lee, Y. J. (2024). Deep learning-based anomaly detection in acceleration data of long-span cable-stayed bridges.

Smart Structures and Systems, An International Journal, 33(2), 93-103. https://doi.org/10.12989/sss.2024.33.2.093

Owen, M. M., Achukwu, E. O., Shuib, S. B., Ahmad, Z. R., Abdullah, A. H., & Ishiaku, U. S. (2023). Effects of high-temperature optimization and resin coating treatment on the mechanical, thermal, and morphological properties of natural kenaf fiber-filled engineering plastic composites. Polymer Composites, 44(4), 2512-2529. https://doi.org/10.1002/pc.27260

Pham, V. T., Thai, D. K., & Kim, S. E. (2025). A novel procedure for cable damage identification of cable-stayed bridge using particle swarm optimization and machine learning. Structural Health Monitoring, 24(2), 714-737. https://doi.org/10.1177/14759217241246501

Sohail, A. (2023). Genetic algorithms in the fields of artificial intelligence and data sciences. Annals of Data Science, 10(4), 1007-1018. https://doi.org/10.1007/s40745-021-00354-9

Su, J., Lai, Q., Hu, J., Xu, L., Xie, L., & Zou, Y. (2025). Optimization of the ground motion intensity measure for long-span suspension bridges considering the impulse effect. Hightech and Innovation Journal, 6(1), 91-103. https://doi.org/10.28991/hij-2025-06-01-07

Tian, Z., Cai, Y., Peng, W., & Wang, Q. (2024). Multi-loop nesting algorithm and response analysis of cable forces of long span cantilever cast arch bridges during construction. KSCE Journal of Civil Engineering, 28(2), 699-714. https://doi.org/10.1007/s12205-023-1970-3

Xiong, W., Diaw, I., Zhu, Y., Zhang, H., & Cai, C. S. (2024). Spatial shape identification of long-span suspension bridges using 3d laser scanning technology. Journal of Civil Structural Health Monitoring, 14(2), 383-400. https://doi.org/10.1007/s13349-023-00732-2

Yin, Z., Wang, J., Wang, T. Y., & Zhu, D. (2022). Optimum design of the long-span continuous steel truss rail beams of straddle monorails. The Journal of Engineering, 2022(12), 1149-1161. https://doi.org/10.1049/tje2.12195

Yu, M., Yao, X., Deng, N., Hao, T., Wang, L., & Wang, H. (2023). Optimal cable force adjustment for long-span concrete-filled steel tube arch bridges: Real-time correction and reliable results. Buildings, 13(9), 2214. https://doi.org/10.3390/buildings13092214

Zhao, T., Tong, W., & Mao, Y. (2022). Hybrid nonsingleton fuzzy strong tracking Kalman filtering for high precision photoelectric tracking system. IEEE Transactions on Industrial Informatics, 19(3), 2395-2408. https://doi.org/10.1109/TII.2022.3160632

Disclaimer